Numerical Simulation of Hydrogen Air Supersonic Coaxial Jet

Malsur Dharavath, Pulinbehari Manna & Debasis Chakraborty

Journal of The Institution of Engineers (India): Series C
Mechanical, Production, Aerospace and Marine Engineering

ISSN 2250-0545
Volume 98
Number 5

J. Inst. Eng. India Ser. C (2017)
98:575-585
DOI 10.1007/s40032-016-0291-4

Springer

J. Inst. Eng. India Ser. C (October 2017) 98(5):575–585
DOI 10.1007/s40032-016-0291-4

ORIGINAL CONTRIBUTION

Numerical Simulation of Hydrogen Air Supersonic Coaxial Jet

Malsur Dharavath[1] · Pulinbehari Manna[1] · Debasis Chakraborty[1]

Received: 18 September 2014 / Accepted: 18 May 2016 / Published online: 18 June 2016

Abstract In the present study, the turbulent structure of coaxial supersonic H_2–air jet is explored numerically by solving three dimensional RANS equations along with two equation k–ε turbulence model. Grid independence of the solution is demonstrated by estimating the error distribution using Grid Convergence Index. Distributions of flow parameters in different planes are analyzed to explain the mixing and combustion characteristics of high speed coaxial jets. The flow field is seen mostly diffusive in nature and hydrogen diffusion is confined to core region of the jet. Both single step laminar finite rate chemistry and turbulent reacting calculation employing EDM combustion model are performed to find the effect of turbulence-chemistry interaction in the flow field. Laminar reaction predicts higher H_2 mol fraction compared to turbulent reaction because of lower reaction rate caused by turbulence chemistry interaction. Profiles of major species and temperature match well with experimental data at different axial locations; although, the computed profiles show a narrower shape in the far field region. These results demonstrate that standard two equation class turbulence model with single step kinetics based turbulence chemistry interaction can describe H_2–air reaction adequately in high speed flows.

Keywords Reacting flow · CFD · Combustion modeling

✉ Debasis Chakraborty
debasis_cfd@drdl.drdo.in; debasis_drdl@yahoo.co.in

[1] Defence Research and Development Laboratory, Hyderabad 500058, Telangana, India

Introduction

The success of efficient design of transatmospheric hypersonic vehicle depends largely on the proper choice of the propulsion system and supersonic combustion Ramjet (scramjet) propulsion is a preferred option. Fluid dynamics and chemistry interact strongly inside the scramjet combustor. Starting from pioneering work of Ferri [1], enormous flow investigations are performed in various countries on different aspects of scramjet flow field including ignition, flame holding, fuel injection, intake combustor interaction etc for both hydrogen and kerosene fuels. Curran [2] identified two emerging scramjet applications namely (i) hydrogen fueled engine to access space and (ii) hydrocarbon-fueled engines for air-launched missiles. Different injection schemes like cavity, strut, pylon for different geometrical configurations and flow conditions are investigated extensively in the last few decades. Since, realistic combustor entrance conditions are hard to achieve in ground test facilities and flight tests are extremely expensive, Computational Fluid Dynamics (CFD) techniques are increasingly being employed for the development of supersonic combustion ramjet (scramjet) propulsion system. The tested and validated numerical codes may bridge the gap between the available experience with subscale combustors and real size engines.

Supersonic combustion with hydrogen fuel is studied extensively both experimentally [3–6] and numerically [7–12] in the literature. These studies mostly measure and compare the wall properties (surface pressure and heat flux) and exit profiles for various flow parameters. Detailed diagnostics of flow distribution, namely; temperature and species mass fraction across a cross section inside the combustor is very limited. To validate high speed reacting flow simulation, it is very much essential to obtain

simultaneous measurement of both fluid dynamical (velocities, temperature etc) and species mass fraction across a plane. Simultaneous measurements of temperature and multi-species concentrations help to study turbulence-chemistry interactions. Temperature and major species concentrations can be used to calculate a reaction scalar that describes the extent of reaction and the local state of fuel/air.

The flowfield within a scramjet combustor is characterized by the interaction of several physical processes including turbulent fuel-air mixing and combustion. Reacting flowfields are described by the Navier–Stokes equations augmented with appropriate species continuity equations that provide for the convection, diffusion, and production of each chemical species. The finite rates of reaction can be accounted for by introducing a multistep chemistry model to describe the reaction mechanism and then applying the law of mass action to determine the rates of production for each species. Chemistry and very fine, high aspect-ratio grid cells near solid walls make the set of governing equations numerically stiff which require a large computational times. To keep the computational effort in a tractable level, the number of chemical species is kept as low as possible. On the other hand, small (skeletal) reaction mechanisms may not be able to accurately predict the lift-off heights of flames at conditions close to the ignition limit. Therefore, skeletal or even one-step schemes should be used with care. The debate on the use of detailed chemistry vis a vis single step chemistry is not adequately resolved in the literature. Number of finite rate chemistry mechanism including Jachimowski mechanisms from 1988 [13] and 1992 [14], Vajda et al. [15], O'Conaire et al. [16] and GRI3.0 [17], abridged Spark model [18] etc. are used to predict the H_2–air reaction in high speed flows. With the exception of the skeletal Jachimowski scheme [19] and the one-step mechanism of Marinov et al. [20] all mechanisms use nine species (H_2, O_2, N_2, H_2O, OH, H, O, HO_2, and H_2O_2), but differ in their number of reactions. In most of the studies, although turbulence closure is employed, turbulence—chemistry interaction was not modelled. Gerlinger et al. [21] compared different chemical schemes to assess their predictive capabilities for high speed reacting flows.

Simultaneous measurement of temperature and species concentration in high speed reacting flow has made the Cheng et al. [22, 23] experiment very special in supersonic reacting code validation and many authors [18, 24–30] has taken this experiment a validation case for their numerical studies. In the experiment of Cheng et al. [22, 23], a pure hydrogen jet is injected at sonic speed into a vitiated supersonic $(M_a = 2)$ coflow. The temperature of the hydrogen is 545 K and the temperature of the hot vitiated air (obtained by precombustion) is 1250 K. Coherent Anti–Stokes Raman Spectroscopy (*CARS*) and Laser Doppler Velocimetry (*LDV*) techniques were used to study the parallel injection of hydrogen fuel in a scramjet combustor. Though this flowfield does not possess the complexities arising from the geometry of a scramjet combustor, nevertheless, it does possess the fundamental physical interaction of a turbulent flow mixing and burning within a chemically reacting environment. Calculations with different chemical schemes for this experimental condition presented in the literature [21] did not make remarkable improvement in the mean temperature in the flow field. Also, most of the studies carried out in the literature did not take into account the fluctuating species flow field caused by turbulence in the combustion process. The fluctuation in the flow field caused by turbulence can significantly alter the oxidiser and fuel distribution and hence reaction process. Number of validation studies carried out by the present authors [24–27] demonstrated that standard two equation class turbulence model with single step kinetics based turbulence chemistry interaction can describe H_2–air reaction adequately in high speed flows. In this paper, Chang et al. experiment [22, 23] is numerically explored with both laminar chemistry and single step kinetics based combustion model to study the effect of turbulence chemistry interaction in high speed H_2–air reacting flow.

Experimental Condition for which the Simulation is Carried Out

A schematic diagram of the flow geometry is taken from Ref [4] and is shown in Fig. 1. The supersonic burner provides an annular, axisymmetric jet of hot, vitiated air of Mach 2. This annular air jet is concentric to the choked main H_2 fuel jet. The exit Reynolds number of the central jet is 15,600. Secondary hydrogen is injected into the combustion chamber directly through four injectors (only one of which is shown in the figure), and oxygen enriched air is distributed at the base of the heater. The stagnation temperature is raised to the required level by burning hydrogen with oxygen enriched air. The vitiated air is accelerated through a convergent-divergent nozzle, exiting into the atmosphere. The walls of the divergent portion of the convergent-divergent nozzle are conical, with a 4.3° half angle. The exit diameter of the vitiated air nozzle is 17.78 mm and the flow accelerate from 1.665 to 2.0 at nozzle exit. The inner and outer diameters of the hydrogen nozzle are 2.36 and 3.88 mm respectively. The combustion of the main hydrogen fuel and the vitiated air forms the supersonic flame. The combustion chamber and the fuel injector are water cooled, and the flow rates of all four gases (hydrogen, air, oxygen, and fuel) are monitored by critical orifices and are controlled by air actuated needle valves. The parameters and operating conditions of the flow are given in Table 1.

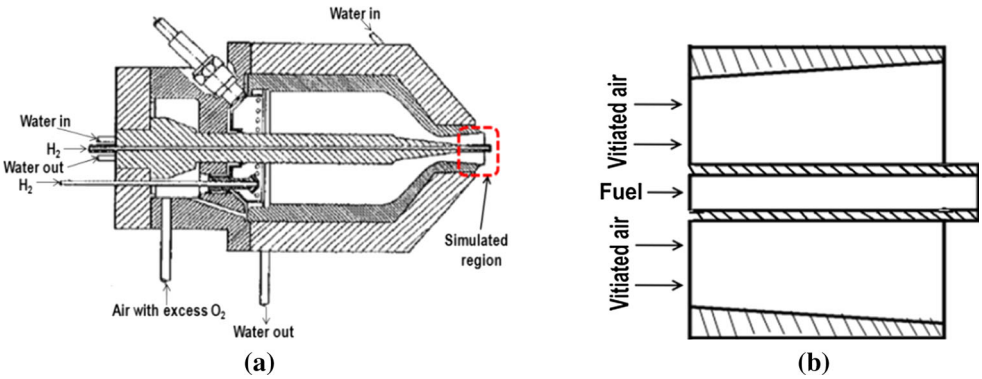

Fig. 1 **a** Schematic diagram of supersonic burner **b** blown up view of simulated nozzle

Table 1 Inflow conditions of the air stream and the hydrogen jet

Parameters	Air (at nozzle inlet)	Hydrogen
Mach number	1.665	1.0
Static pressure (kPa)	172.22	112
Static temperature (K)	1233	545
Axial velocity (m/s)	1188	1780
O_2 mol fraction	0.201	0.0
H_2O mol fraction	0.225	0.0
N_2 mol fraction	0.544	0.0
H_2 mol fraction	0.000	1.0

Computational Methodology

Three-dimensional Reynolds Averaged Navier Stokes (RANS) equations are solved using commercial CFD code CFX [28] which is an integrated software system capable of solving diverse and complex multidimensional fluid flow problems. The code is fully implicit, finite volume method with finite element based discretization of geometry. The method retains much of the geometric flexibility of finite element methods as well as the important conservation properties of the finite volume method. It utilizes numerical upwind schemes to ensure global convergence of mass, momentum, energy and species. It implements a general non-orthogonal, structured, boundary fitted grids. The convective terms are discretized through 2nd order scheme and k-ε turbulence model with wall functions was used in present simulations.

Combustion Modeling

The single-step global kinetics scheme is adopted in light of its simplicity and reasonably accurate modelling of the burned gas containing completely oxidized species of hydrogen (H_2) fuel. The scheme for H_2–oxidation involves the following one steps (global step) reaction and three species:

$$2H_2 + O_2 \rightarrow 2H_2O$$

The effect of turbulent mixing on combustion is taken into account by means of the *eddy-dissipation model* (*EDM*) [29]. In this model, the chemical reaction is fast relative to the transport process in the flow. When, reactants mix at the molecular level they instantaneously form products. The model assumes that the reaction rate may be related directly to the time required to mix reactants at molecular level. In turbulent flows, this mixing time is dictated by the eddy properties and therefore the burning rate is proportional to the rate at which turbulent kinetic energy is dissipated i.e., reaction rate $\alpha\ \varepsilon/k$, where k is the turbulent kinetic energy and ε is its rate of dissipation. The reaction rate associated with turbulent mixing, is given by the minimum of the following three rates

$$R_{\mathrm{H}_2,edm} = A_{ed}\overline{\rho}\frac{\varepsilon}{k}\min\left\{Y_f, \frac{Y_o}{\nu_{\mathrm{H}_2}}, B_{ed}\frac{Y_p}{1+\nu_{\mathrm{H}_2}}\right\}$$

where, Y_f, Y_o and Y_p are the mass fraction of fuel, oxidant and products respectively, A_{ed} and B_{ed} are empirical constants taken to be 4.0 and 0.5, respectively, ν_{H_2} is stoichiometric coefficients of H_2 reaction.

In *Laminar Finite Rate Chemistry Model (LFRCM)* the kinetic rate of change of any species (H_2, O_2 and H_2O) in a reaction is generally described by an Arrhenius expression involving an exponential dependence on temperature and power law dependence on the concentrations of the reacting chemical species. The rate of reaction of $R_{\mathrm{H}_2,frc}$ (in kg-mol/m^3 s) is given by the expression [30, 31],

$$R_{\mathrm{H}_2,frc} = -2\left\{1.102\times10^{19} * \exp(-8052/T)c_{\mathrm{H}_2}^2 c_{\mathrm{O}_2} - \kappa_b c_{\mathrm{H}_2\mathrm{O}}^2\right\}$$

where, c is the molar concentration (in g-mol/cm^3) and κ_b, the rate constant of backward reaction, is obtained from the forward rate constant and equilibrium constant ($\kappa_b = \kappa_f/\kappa_e$), where κ_f and κ_e are forward rate constant and the equilibrium coefficient respectively, it can be written as; $\kappa_e = (RT)^{-2}\exp(-2g_i/RT)$. The finite rate turbulence chemistry interaction (*TCI*) is difficult to model and needs extra source term for the prediction of *TCI*. Such interactions are not considered in the present study.

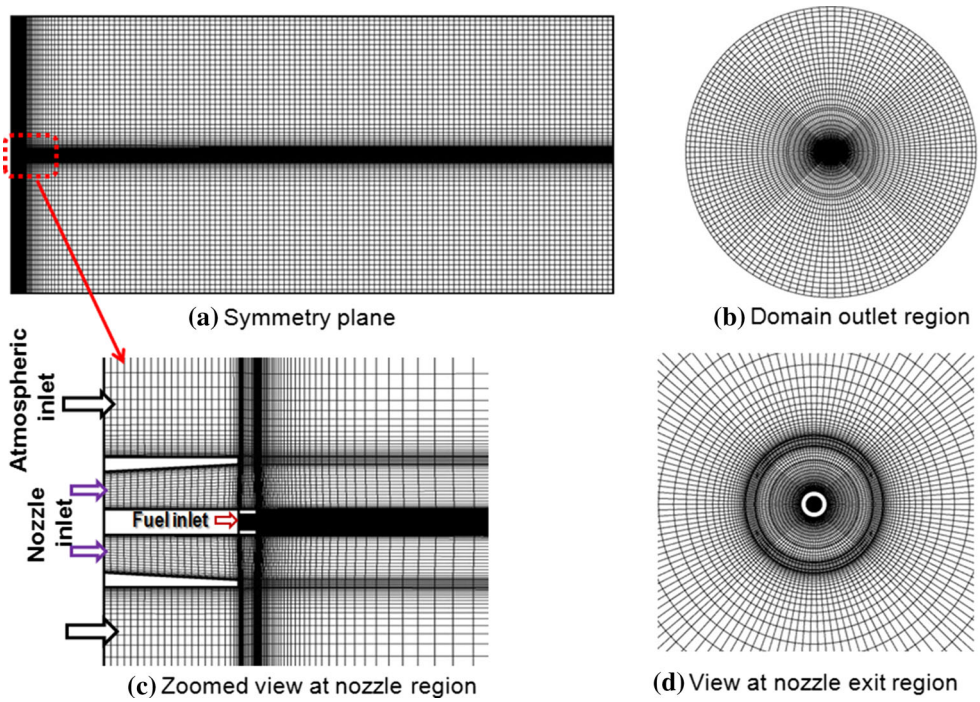

Fig. 2 Typical grid distribution on various planes (Total grid size ~2.84 millions)

Results and Discussions

Grid Independence Study

A structured grid involving 2.84 million points are generated in the computational domain. Typical grid distribution in the symmetry plane alongwith the zoomed view around the fuel and vitiated air nozzles are shown in Fig. 2. The grid is made very fine at the walls of the nozzle and near the interface between the vitiated air and hydrogen fuel jet and is stretched exponentially in radial outward directions. Y^+ value near nozzle wall is of the order of 1. The computational domain is extended to 650 D in the downstream direction and ± 150 D in radial direction (where, $D = 2.36$ mm is the hydrogen jet diameter). Two different grids of size $430 \times 75 \times 75$ (coarse) and $550 \times 90 \times 90$ (fine) are employed to find out the grid independence of the results. The jet centerline pressure distributions for these two grid are compared in Fig. 3 and a close match between the two is observed. An error estimate due to grid is also presented in the figure. For steady state boundary -value problem, the main source of numerical error in *CFD* is iterative convergence or grid convergence error [32]. The simplest of such estimate is given by the relative difference $\varepsilon = (f_1 - f_1)/f_1$ [33], where, f represent any quantity of interest and the indices 1 and 2 refer to the fine and coarse grid solution respectively. (In the present calculation, the centerline pressure is taken as the parameter of interest) Roache [34] has proposed a grid-convergence index (*GCI*) as an error

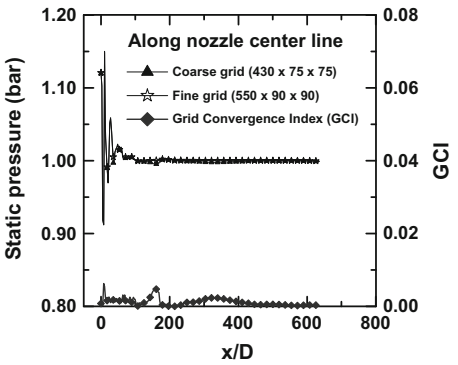

Fig. 3 Grid independence and grid convergence index

based on uncertainty estimate of the numerical solution as,

$$GCI = F_s \frac{1\varepsilon 1}{(h_2/h_1)^p - 1}$$

where, h is the order of grid spacing, p is the order of accuracy of numerical scheme and F_s is a factor of safety. Roache [35] has suggested $F_s = 3$ for minimal of two grid calculations. For the present calculation p is equal 2 with h_2/h_1 equal 2, *GCI* is order of ε. Aswin and Chakraborty [36] have already used this estimate to grid convergence error for transverse sonic jet interaction in supersonic free stream. Maximum error between two grids is less than 1 %. This analysis indicates that the grid is adequate to capture most of features of the flow and the solution in grid independent. Simulations are carried out

with fuel injection both for cold flow (nonreacting) and hot (reacting) flow. Velocity, pressure and temperature conditions are imposed at vitiated air nozzle and sonic conditions are prescribed for hydrogen injector exit. Atmospheric pressure of 1 bar is prescribed at atmospheric inlet and radial and outflow boundaries. Log-normalized maximum residue of −04 is considered as the convergence criteria.

Flow Field Analysis with EDM

Two sets of steady state reacting flow calculations are carried out using (i) Eddy Dissipation Model (EDM) and (ii) Single step laminar finite rate chemistry (LFRCM) for quantitative estimation of turbulence—chemistry interaction. The Mach number, temperature, oxygen (Y_{O_2}) and water (Y_{H_2O}) mass fractions distributions at different axial planes *P1–P10* (i.e., $x = 0.01$, 0.03, 0.05, 0.07, 0.09, 0.11, 0.13, 0.15, 0.17 and 0.19 m) are presented in Fig. 4a–d to depict the qualitative features of mixing of two supersonic jets in turbulent reacting environment. Hydrogen mass fraction in the nozzle centre is also superimposed in water mass fraction distribution (Fig. 4d). The simulation captures all the pertinent features of the flow field. Mach number in the core of the jet is reduced because of heat release due to reaction (Fig. 4a). From the temperature (Fig. 4b) and water mass fraction distribution (Fig. 4c), it is clear that most of the reactions are occurring at the core of the jets. Hydrogen fuel is seen to diffuse very little in the radial direction. At the core, hydrogen diminishes gradually along the length and almost less than 0.5 % is available at x = 0.17 m apart from the base of the nozzle. High momentum of the coflowing vitiated air (65.58 kg m/sec) compared to fuel jet (0.345 kg m/sec) is mainly responsible for slow spreading of hydrogen jet in radial direction. Due to reaction, oxygen is almost fully consumed in the core at vicinity to the base. However, in the downstream due to mixing with the coflow jet, Y_{O_2} increases at the core (Fig. 4c). The composite picture of Y_{H_2} mass fraction from center and streamwise vorticity contours (non-dimensionalised with $\Omega_{zref} = 80000$ [1/s]) at different axial locations is shown in Fig. 5. It is observed that, streamwise vorticity decreases with downstream distance from nozzle exit due to mixing with surrounding air.

The mixing effectiveness formulation assumes the least available reactant, fuel or air. The other reactant is considered completely mixed already. For instance, in a fuel-lean situation as is the present case, the fuel is the concern for mixing. Air is considered to be completely mixed. The mixing efficiency (η_m) is defined as [37],

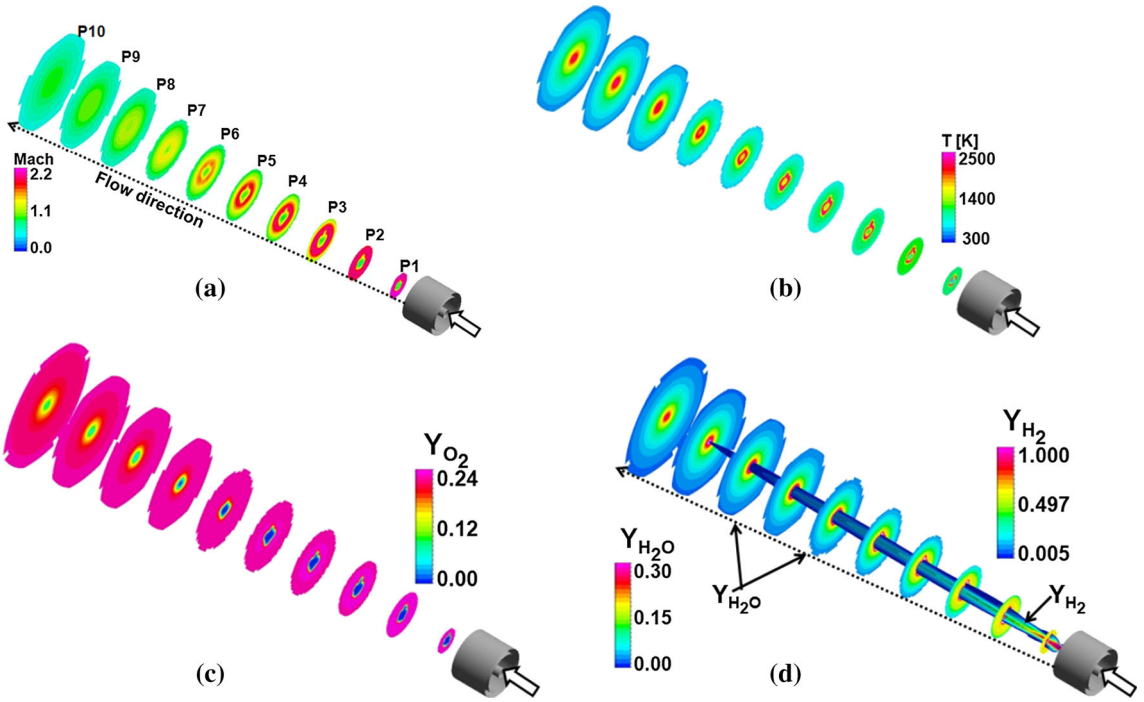

Fig. 4 Contours at different axial locations of the flow field (**a**) Mach number, (**b**) Static temperature, (**c**) Oxygen mass fraction and (**d**) Composite picture of water mass fraction (axial locations) and hydrogen mass fraction (nozzle center)

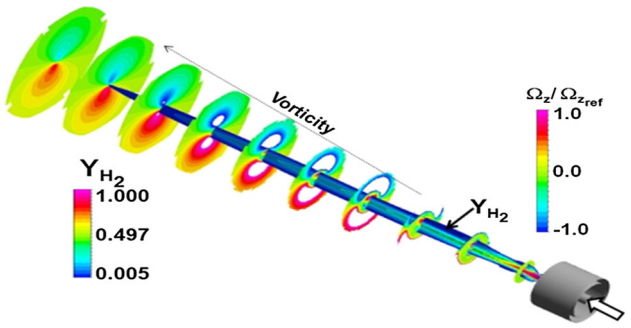

Fig. 5 Composite picture of streamwise vorticity contours (axial locations) and hydrogen mass fraction (center of nozzle)

$$\eta_m(x) = \frac{\int A\alpha_{gas} Y_{H_2} u dA}{\dot{m}_{H_2}(x)}$$

$$\text{with } \alpha = \begin{cases} \frac{1}{\emptyset} : \emptyset \geq 1, \\ 1 : \emptyset < 1 \end{cases}$$

where ρ_{gas} is the gas density, Y_{H_2} is the mass fraction of hydrogen, A is the cross-sectional area and u is the axial velocity. Here, $\emptyset$ is the local equivalence ratio and is defined as:

$$\emptyset = \frac{1}{2}\frac{M_{O_2}}{M_{H_2}}\frac{Y_{H_2}}{Y_{O_2}}$$

with M_{H_2} and M_{O_2} are the molecular weights of hydrogen and oxygen respectively, and Y_{O_2} is the mass fraction of oxygen.

The combustion efficiency (η_c), which describes how much of the injected fuel has been consumed, is defined by **[37],**

$$\lambda_c(x) = 1 - \frac{\int A_{gas} Y_{H_2} u dA}{\dot{m}_{H_{2,inj}}}$$

The mixing and combustion efficacy distribution along the length of the flow is shown in Fig. 6. It is observed that, mixing and combustion become complete within the range of $0 < X < 0.35$ m from nozzle exit.

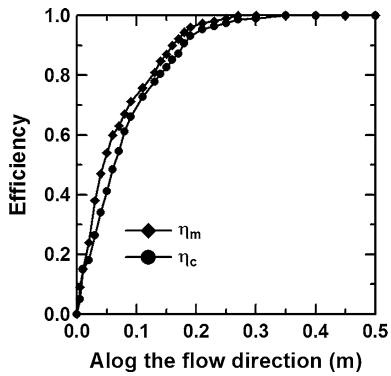

Fig. 6 Comparison of mixing and combustion efficiencies along the flow directions

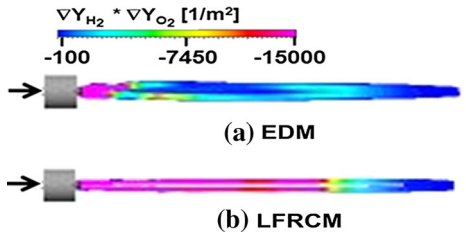

Fig. 7 Distribution of $\nabla Y_{H_2} * \nabla Y_{O_2}$ near injection region

Comparison of EDM versus LFRCM Results

To find out the region of premixed and diffusion dominated combustion, the distribution of the term $\nabla Y_{H_2} * \nabla Y_{O_2}$ in the symmetry plane is presented in Fig. 7. Chakraborty et al. [30] used this index to determine the zone of premixed and diffusion combustion in the mixing layer. The basic idea is that if the dot product of the gradient of fuel and oxidizer mass fraction is strongly negative, then the zone is dominated by diffusive combustion since the flame is fed by the oxidizer and fuel from opposite direction; if the quantity is strongly positive, the zone is affected by premixed combustion since the fuel and oxidizer is fed from the same side. From the figure it is clear that near the injection and mixing zone is burning is mostly diffusive in nature. For laminar flame, the diffusive zone is much more intense. Damkohler number $\left(\left\{\frac{w_{H_2}}{\rho Y_{H_2}}\right\}/\left\{\frac{V}{L}\right\}\right)$ distribution near the injector is shown in Fig. 8. Since turbulence chemistry interaction makes reaction rate lower, the Damkohler number for EDM simulation is much lower compared to LFRCM. Since the Damkohler number is greater than unity, the reaction is mixing limited and the fast chemistry assumption in the simulation is justified.

Computed hydrogen mole fraction profiles with both the simulations are compared with experimental results [22, 23] at four different axial locations ($x/D = 0.85$, 10.8, 64.7 and 86.1) in Fig. 9. A good match is obtained between the experimental and computational values. Even at much downstream station at $x/D = 64.7$, the comparison between experimental and computational is reasonable. Laminar reaction (*LFRCM*) is showing higher H_2 mol fraction compared to turbulent reaction (*EDM*) because of lower reaction rate caused by turbulence chemistry interaction. The comparisons of computed oxygen mole fraction

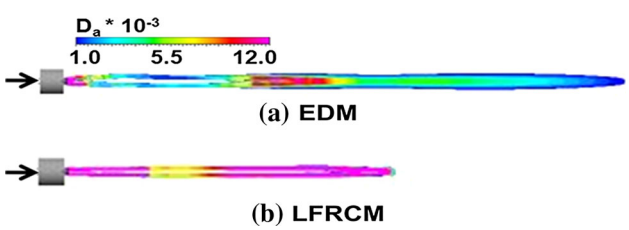

Fig. 8 Damkohler number distribution near injection region

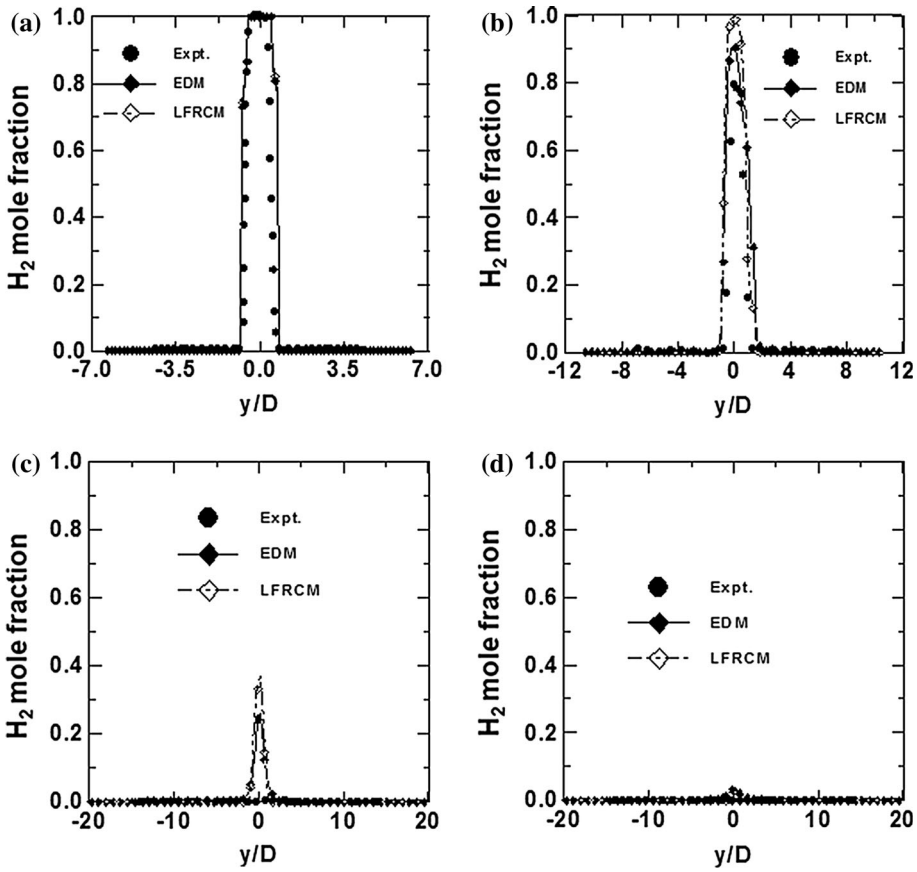

Fig. 9 Comparison of computed H_2 mol fraction with experimental data at different axial locations (**a**) $x/D = 0.85$ (**b**) x/D = 10.8 (**c**) $x/D = 64.7$ and (**d**) $x/D = 86.1$

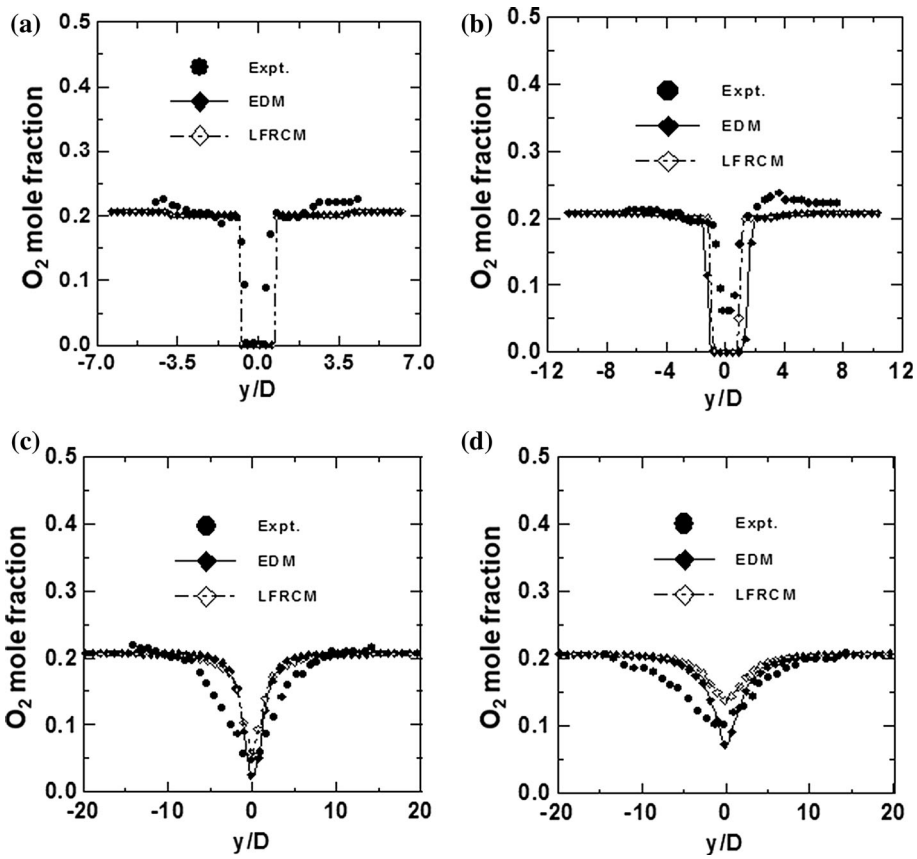

Fig. 10 Comparison of computed O_2 mol fraction with experimental data at different axial locations (**a**) $x/D = 0.86$ (**b**) x/D = 10.8 (**c**) $x/D = 64.7$ and (**d**) $x/D = 86.1$

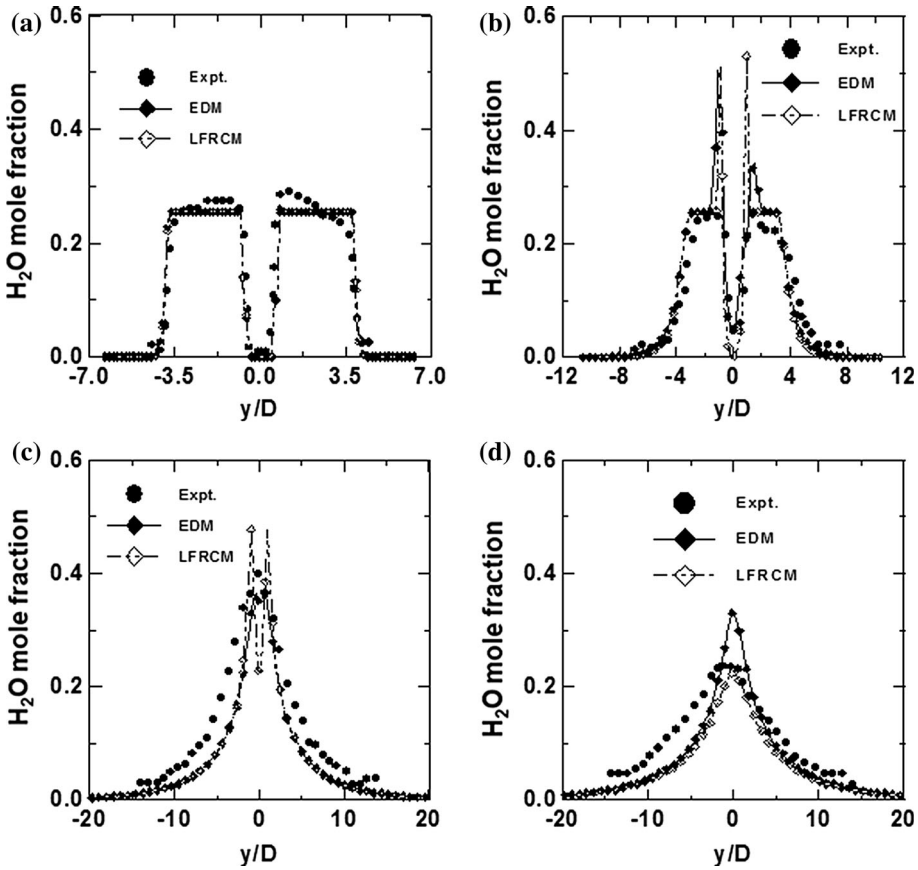

Fig. 11 Comparison of computed H_2O mole fraction profiles with experimental data at different axial locations (**a**) $x/D = 0.86$ (**b**) x/D = 10.8 (**c**) $x/D = 64.7$ and (**d**) $x/D = 86.1$

profiles with experimental results at various axial stations are shown in Fig. 10. A very good match between experiment and computations is obtained for the peak O_2 mol fraction for all axial stations. Although, in the near field (upto $x/D = 10.8$), the computed profile match with the experimental one, in the far field, the computation predicts a narrower shape compared to experimental one. The fickian diffusion model adopted in the simulation may be the cause for this narrow profile. At the farthest station, $x/D = 86.1$, the laminar calculation show lower peak value of O_2 mol fraction compared to both experimental and turbulent calculation. Water mass fraction profile comparison at various axial stations is presented in Fig. 11. The computed water mass fraction profile compare very well with experimental results in the near field, whereas; in the far field, computed water mass fraction profile show slight narrower profile compared to experiment. The computed peak of water mass fraction is higher compared to experimental data because of fast chemistry assumption. Computed water mass fractions with different chemical schemes presented in the literature [21] almost coincide with each other indicating the marginal effect of detailed chemical kinetics for this experimental condition. Present computations also demonstrate that standard two equation class turbulence model with single step kinetics based turbulence chemistry interaction can describe H_2–air reaction adequately in high speed flows. Computed nitrogen mole fraction profiles match very nicely with experimental results in the flow field as shown in Fig. 12. The computed peak value of nitrogen mole fraction in the far field region show slight over-prediction. Computed temperature profiles at various axial stations are compared with experimental results in Fig. 13. Overall good agreement between experiment and computation has been obtained. As observed for other profiles, the computed temperatures also predict a narrower profile compared to experimental data. It is not very clear that whether the fickian diffusion velocity model is having any role in explaining the role of narrower profile obtained in the simulation. The laminar simulations show higher values of peak temperature near the jet axis due to fast reaction compared to turbulent calculation.

Conclusions

Coaxial supersonic reacting flow where sonic hydrogen is injected into central Mach 1.66 jet is simulated numerically by solving three dimensional RANS equations alongwith two equation k–ε turbulence model. Grid independence of

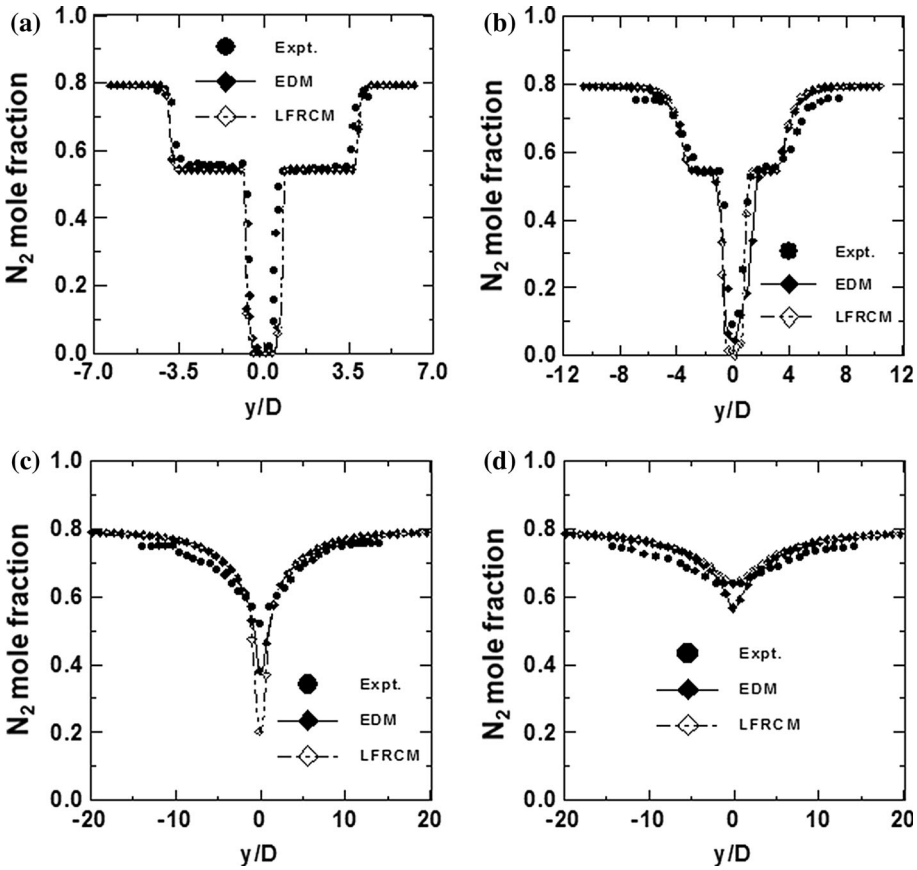

Fig. 12 Comparison of computed N_2 mol fraction profiles with experimental data at different axial locations (**a**) $x/D = 0.86$ (**b**) x/D = 10.8 (**c**) $x/D = 64.7$ and (**d**) $x/D = 86.1$

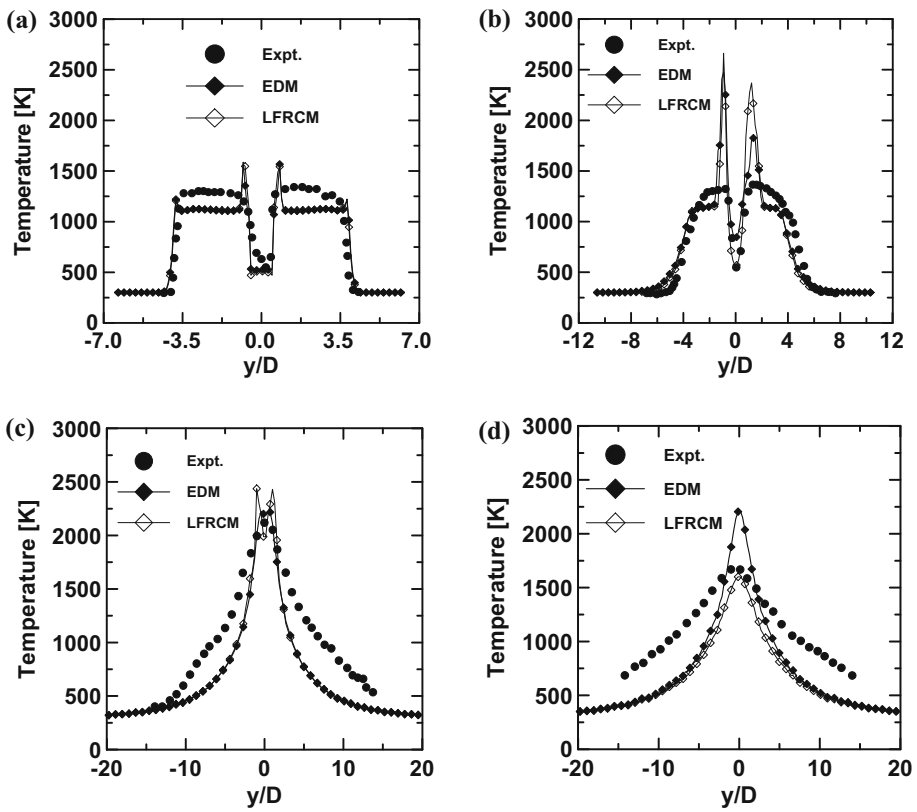

Fig. 13 Comparison of computed temperature profile with experimental data at different axial locations (**a**) $x/D = 0.86$ (**b**) x/D = 10.8 (**c**) $x/D = 64.7$ and (**d**) $x/D = 86.1$

the solution is demonstrated by comparing the results with two different grids as well as estimating the error distribution using Grid Convergence Index. Two sets of reacting calculations are performed using single step laminar finite rate chemistry and EDM based combustion model to find the effect of turbulence-chemistry interaction in the flow field. Simulations capture all essential features of the flow field including the shock structures. The flow field is seen mostly diffusive in nature and hydrogen diffusion is confined to core region of the jet because of high momentum of vitiated air flow. Laminar reaction predicts higher H_2 mol fraction compared to turbulent reaction because of lower reaction rate caused by turbulence chemistry interaction Computed hydrogen, oxygen, nitrogen, water mole fractions and temperature profiles match well with experimental data at different axial locations in the near field and far field regions. In the far field region, the computed profiles show a narrower shape compared to the experimental data. The profiles of major species and temperature compare very well with the data obtained with detailed kinetics available in the literature. These results demonstrate that standard two equation class turbulence model with single step kinetics based turbulence chemistry interaction can describe H_2–air reaction adequately in high speed flows.

References

1. A. Ferri, Review of problems in application of supersonic combustion. J. R. Aeronaut. Soc. **68**(645), 575–597 (1964)
2. E.T. Curran, Scramjet engines: the first forty years. J. Propul. Power **17**(6), 1138–1148 (2001)
3. M. C. Burrows, A. P. Kurkov, Analytical and experimental study of supersonic combustion of hydrogen in vitiated air stream. Report No. NASA-TMX-2828 (1973)
4. T. Cheng, J. Wehrmeyer, R. Pitz, O. Jarrett Jr., G. Northam, Finite rate chemistry effects in a Mach 2 reacting flow. AIAA Paper 91-2320 (1991)
5. J. Erdos, J. Tamagno, R. Bakos, R. Trucco, Experiments on shear layer mixing at hypervelocity conditions. AIAA Paper 1992-0628 (1992)
6. S. Tomioka, A. Murakami, K. Kudo, T. Mitani, Combustion tests of a staged supersonic combustor with a strut. J. Propul. Power **17**(2), 293–300 (2001)
7. J. P. Drummond, Supersonic reacting internal flow field, in *Numerical Approaches in Combustion Modeling,* ed. by E. S. Organ, J. P. Borris, *Progress in Aeronautics and Astronautics,* AIAA, vol 135, p. 365–420 (1991)
8. M. H. Carpenter, Three dimensional computations of cross flow injection and combustion in a supersonic flow, AIAA Paper 1989–1870 (1989)
9. K. Uenishi, R. C. Rogers, G. B. Northam, Three dimensional computation of transverse hydrogen jet combustion in a supersonic air stream, AIAA Paper 1987-0089 (1987)
10. T. Chitsomboon, G.B. Northam, Computational fluid dynamics prediction of the reacting flowfield inside a subscale scramjet combustor. J. Propul. Power **7**, 44–48 (1991)
11. S. Saha, D. Chakraborty, Reacting flow computation of staged supersonic combustor with strut injection. AIAA Paper No. 2006-3895 (2006)
12. S.W. Kim, Numerical investigation of chemical reaction—turbulence interaction in compressible shear layer. Combust. Flame **101**, 197–208 (1995)
13. C. J. Jachimowski, An analytical study of the hydrogen–air reaction mechanism with application to scramjet combustion. NASA-TP-2791 (1988)
14. C. J. Jachimowski, An analysis of combustion studies in shock expansion tunnels and reflected shock tunnels. NASA-TP-3224 (1992)
15. S. Vajda, H. Rabitz, R.A. Yetter, Effects of thermal coupling and diffusion on the mechanism of H_2 oxidation in steady premixed laminar flames. Combust. Flame **82**, 270–292 (1990)
16. M. O'Conaire, H.J. Curran, J.M. Simmie, R.W. Pitz, C.G. Westbrook, A comprehensive modeling study of hydrogen oxidation. Int. J. Chem. Kinet. **11**, 602–622 (2004)
17. G. P. Smith, D. M. Golden, M. Frenklach, N. W. Moriarty, B. Eiteneer, M. Goldenberg, C. T. Bowman, R. K. Hanson, S. Song, W. C. Gardiner, V. V. Lissianski, Z. Qin, GRI3.0 mechanism (1995), Available from:http://www.me.berkeley.edu/grimech/
18. D.R. Eklund, J.P. Drummond, H.A. Hassan, Calculation of supersonic turbulent reacting coaxial jet. AIAA. J. **28**, 1633–1641 (1990)
19. R. L. Gaffney, J. A. White, S. S. Girimaji, J. P. Drummond, Modeling turbulent/chemistry interactions using assumed PDF methods. AIAA Paper 1992-3638 (1992)
20. N.M. Marinov, C.K. Westbrook, W.J. Pitz, Detailed and global chemical kinetics model for hydrogen, in *Proceedings of the Eighth International Symposium on Transport Phenomena in Combustion*, ed. by S.H. Chan (Taylor and Francis, London, 1995), pp. 118–129
21. P. Gerlinger, K. Nold, M. Aigner, Influence of reaction mechanisms, grid spacing, and inflow conditions on the numerical simulation of lifted supersonic flames. Int. J. Numer. Meth. Fluids **62**, 1357–1380 (2010)
22. T. Cheng, J. Wehrmeyer, R. Pitz, O. Jarrett Jr., G. Northam, Finite-rate chemistry effects in a mach 2 reacting flow. AIAA Paper 1991–2320 (1991)
23. T.S. Cheng, J.A. Wehrmeyer, R.W. Pitz, O. Jarrett, G.B. Northam, Mixing enhancement in compressible mixing layers:an experimental study. Combust. Flame **99**, 157–173 (1994)
24. M.S.R. Chandra Murty, D. Chakraborty, Effect of injection angle in mixing and combustion characteristics of scramjet combustor. Int. J. Hypersonics **2**(1–2), 15–27 (2011)
25. R. Ingle, D. Chakraborty, Numerical simulation of dual mode scramjet combustor with significant upstream interaction. Int. J. Manuf. Mater. Mech. Eng. **2**(3), 60–74 (2012)
26. MSR Chandra Murty and Debasis Chakraborty, Numerical simulation of angular injection of hydrogen fuel in scramjet combustor. J. Aerosp. Eng. **226**(7), 861–872 (2012)
27. M. Dharavath, P. Manna, D. Chakraborty, Thermochemical exploration of hydrogen combustion in generic scramjet combustor. Aerosp. Sci. Technol. J. **24**, 264–274 (2013)
28. ANSYS-CFX, Release 11.0: Installation and Overview, 7 July 2007
29. B. F. Magnussen, B. H. Hjertager, On mathematical modeling of turbulent combustion with special emphasis on soot formation and combustion, In: Sixteenth Symp. (Int.) on Combustion, The Combustion Institute, Pittsburg, pp. 719–729 (1976)
30. Debasis Chakraborty, H.V. Nagraja Upadhaya, P.J. Paul, H.S. Mukunda, A thermo-chemical exploration of two dimensional reacting supersonic mixing layer. Phys. Fluids **9**(11), 3513–3522 (1997)
31. Debasis Chakraborty, P.J. Paul, H.S. Mukunda, Evaluation of empirical combustion models for high speed H_2/air confined

mixing layer using DNS data. Combust. Flame **121**, 195–209 (2000)
32. AIAA Standard, *Guide for the Verification and Validation of Computational Fluid Dynamic simulation G-077-1998* (AIAA, Reston, VA, 1998)
33. A. D. Cutler, P.M. Danehy, S. O'Byrne, C. G. Rodrigues, J .P. Drummond, Supersonic combustion experiment for CFD model development and validation. AIAA Paper No. 2004-266 (2004)
34. P. J. Roache, Error base for CFD. AIAA Paper No. 2003-0408 (2003)
35. P.J. Roache, *Verification and Validation in Computational Science and Engineering* (Hermon Publishers, Albuquerque, 1998)
36. G. Aswin, Debasis Chakraborty, Numerical simulation of transverse side jet interaction with supersonic free stream. Aerosp. Sci. Technol. J. **14**, 295–301 (2010)
37. T. Shuhei, W. Kazunori, T. Sadatake, T. Mitsuhiro, K. Michikata, Effects of combustion on flowfield in a model scramjet combustor. Twenty-Seventh Symposium (International) on Combustion, The Combustion Institute, pp. 2143–2150 (1988)